THE JOURNAL OF BIOLOGICAL CHEMISTRY VOL. 287, NO. 20, pp. 16238–16245, May 11, 2012

Post-translational Modifications Regulate Assembly of Early Spindle Orientation Complex in Yeast*[S]

Received for publication, January 30, 2012, and in revised form, March 15, 2012 Published, JBC Papers in Press, March 29, 2012, DOI 10.1074/jbc.M112.347872

Daniela Hüls[‡§], **Zuzana Storchova**[¶], **and Dierk Niessing**[‡§1]

From the [‡]*Institute of Structural Biology, Helmholtz Zentrum München-German Research Center for Environmental Health, 85764 Neuherberg, the* [§]*Gene Center and Department of Biochemistry, Ludwig-Maximilians University, 81377 Munich, and the* [¶]*Group Maintenance of Genome Stability, Max Planck Institute of Biochemistry, 82152 Martinsried, Germany*

Background: Mitotic spindle orientation in budding yeast is achieved by a motor complex consisting of Myo2p, Kar9p, and Bim1p.
Results: Interaction of Kar9p with Bim1p requires Kar9p sumoylation and is impaired by Bim1p phosphorylation.
Conclusion: Assembly of the spindle orientation complex is regulated by sumoylation and phosphorylation of its core factors.
Significance: Orientation of the mitotic spindle is an essential feature of cell division.

Mitosis begins with the tethering of chromosomes to the mitotic spindle and their orientation perpendicular to the axis of cell division. In budding yeast, mitotic spindle orientation and the subsequent chromosome segregation are two independent processes. Early spindle orientation is driven by the actin-bound myosin Myo2p, which interacts with the adapter Kar9p. The latter also binds to microtubule-associated Bim1p, thereby connecting both types of cytoskeleton. This study focuses on the interaction between Kar9p and Bim1p and its regulation. We solved the crystal structure of the previously reported Kar9p-binding motif of Bim1p and identified a second, novel Kar9p interaction domain. We further show that two independent post-translational modification events regulate their interaction. Whereas Kar9p sumoylation is required for efficient complex formation with Bim1p, Aurora B/Ipl1p-dependent phosphorylation of Bim1p down-regulates their interaction. The observed effects of these modifications allow us to propose a novel regulatory framework for the assembly and disassembly of the early spindle orientation complex.

During mitosis, chromosomes associate with kinetochore microtubules and are subsequently segregated. Before segregation can occur, the spindle has to be oriented correctly in the cell to ensure equal distribution of the chromosomes between mother and daughter cells. In budding yeast, proper alignment of the mitotic spindle prior to anaphase relies on a myosin-dependent transport event along actin filaments (1–3). It is followed by a second, partially redundant, dynein-dependent spindle elongation event during anaphase (3).

For spindle alignment in pre-anaphase, the highly conserved type V myosin motor Myo2p interacts with the adapter Kar9p (karyogamy 9 protein), which itself binds to the microtubule-associated Bim1p (binding to microtubules 1 protein) (1). Whereas Kar9p shows weak homology to the adenomatous polyposis coli (APC)[2] tumor suppressor (3–5), Bim1p is a member of the highly conserved EB1 (end-binding protein 1) family of proteins that are known to bind microtubules (6). In humans, mutations in APC are responsible for development of familial adenomatous polyposis and resulting colorectal cancer (7). Its binding partner EB1 has been identified as a prognostic marker for recurrence and survival of hepatocellular carcinoma (8) and as an oncogenic factor (9).

Human EB1 shares 35% sequence identity with its yeast ortholog Bim1p (6). Both contain an N-terminal calponin homology (CH) domain and an EB1-like C-terminal motif, separated by a linker region. The CH domain is highly conserved and mediates binding to microtubules (10). The EB1 homolog Mal3p from *Schizosaccharomyces pombe* decorates microtubules along the lattice seam in a zipper-like manner (11).

In humans, the C-terminal EB1-like motif is sufficient to bind to a peptide of the APC protein (12, 13). Likewise, in yeast, the EB1-like domain of Bim1p is sufficient to bind to Kar9p (14). Crystal structures of the CH domain from yeast and humans (10, 15) and of the EB1 motif from human EB1 (12, 13) have been determined. No structure is available for the yeast EB1-like motif.

The linker region between the CH and EB1-like domains contains no structurally defined domain. In yeast, this linker region of Bim1p is the target of cell cycle-dependent phosphorylation by Aurora B/Ipl1p and supports the microtubule binding of the CH domain (16). Also human EB1 interacts with Aurora B kinase (17), suggesting conservation of this post-translational modification.

Because APC is a very large protein (4), only few details are available that explain its molecular function during the cell cycle. In contrast, for its shorter yeast homolog Kar9p, the interaction partners and modifying enzymes have been identi-

* This work was supported by the Helmholtz Association (to D. N.) and the Deutsche Forschungsgemeinschaft (to Z. S. and D. N.).
[S] This article contains supplemental Figs. S1–S6 and Tables S1–S4.
The atomic coordinates and structure factors (code 4E61) have been deposited in the Protein Data Bank, Research Collaboratory for Structural Bioinformatics, Rutgers University, New Brunswick, NJ (http://www.rcsb.org/).
[1] To whom correspondence should be addressed. Tel.: +49-89-3187-2176; E-mail: niessing@helmholtz-muenchen.de.

[2] The abbreviations used are: APC, adenomatous polyposis coli; CH, calponin homology; BisTris, 2-[bis(2-hydroxyethyl)amino]-2-(hydroxymethyl)propane-1,3-diol; MBP, maltose-binding protein.

fied. Kar9p is subject to sumoylation (18, 19) and phosphorylation (2, 20). Although both types of modification are regulated independently, mutations in Kar9p affecting either of them result in impaired spindle orientation (18). To date, it is unclear why these modifications are important.

Here, we provide a mechanistic explanation for how post-translational modifications in Kar9p and Bim1p contribute to the regulation of their functions. We found that unmodified Kar9p fails to bind to Bim1p, whereas Kar9p from yeast extracts efficiently binds to recombinant Bim1p. Pulldown assays with yeast strains expressing Kar9p with mutated sumoylation sites showed severely reduced Bim1p binding. Thus, Kar9p sumoylation is likely required for the efficient assembly of the spindle orientation complex.

We solved the crystal structure of the C-terminal EB1-like domain of Bim1p and generated structure-based mutations that either abolished or increased the interaction with Kar9p. Furthermore, we identified a novel Kar9p interaction region in Bim1p. This region is subject to cell cycle-dependent phosphorylation by the Aurora B kinase, which we found to down-regulate Bim1p binding to Kar9p.

EXPERIMENTAL PROCEDURES

Yeast Strains and Plasmids—General yeast methods were performed as described (21–23). Detailed information on strains and plasmids is provided in supplemental Tables S2–S4. Deletion mutants were obtained by a PCR-based knock-out method (24) and verified by PCR. Mutations of *BIM1* and *KAR9* were introduced by site-directed mutagenesis.

Yeast Growth Conditions—For pulldown experiments, cells were plated on synthetic-complete (SC)-His plates and grown in YPD (yeast extract/peptone/dextrose) at 30 °C until the mid-logarithmic phase. For Kar9p overexpression, cells were grown in YPR (yeast extract/peptone/raffinose) to $A_{600} = 1$ and induced with 2% galactose for 3–4 h at 30 °C. For pulldown experiments with His-tagged Smt3p, cells were plated on synthetic complete (SC)-Ura plates and grown in synthetic complete (SC)-Ura and raffinose as described for Kar9p overexpression.

Protein Purification for Crystallization and Pulldown Experiments—GST-tagged Bim1p fragments were expressed in *Escherichia coli* and isolated to high purity using standard chromatographic techniques (25). GST tags were removed by protease cleavage (26) unless stated otherwise. Protein quantities were calculated from their absorbance at 280 nm and individual molar extinction coefficients. Purified Bim1p and Kar9p were stable over days. Crystals were grown at 21 °C by hanging-drop vapor diffusion using a 1:1 mixture of protein (2 mg/ml) and crystallization solution containing 0.1 M BisTris (pH 8.0), 20% PEG 5000 MME, 40% γ-butyrolactone, and 10 mM potassium tetranitroplatinate(II) for heavy atom-soaked crystals. Crystals appeared within 1–2 days. Maltose-binding protein (MBP)-tagged Bim1p was expressed in *E. coli*, affinity-purified via an amylose resin (PerkinElmer Life Sciences), and eluted with 10 mM maltose. Purification was finished by chromatography on a Superose 12 column (GE Healthcare) (27).

Structure Determination—20% ethylene glycol was used as a cryoprotectant. Single anomalous dispersion experiments and native data sets were recorded at beamline ID-29 (European Synchrotron Radiation Facility, Grenoble, France). The data were integrated and scaled using XDS (28). Phases were obtained with SHELX (29). The model was built manually from the platinum data set using Coot (30). The native protein structure was solved by molecular replacement using Phaser (31) with the platinum structure as a search model. Refinement was performed with BUSTER (32) using non-crystallographic symmetry.

Bioinformatics—Sequence alignments were performed with the programs Clustal (European Bioinformatics Institute) and visualized with Jalview. The surface plot of sequence conservation was generated with Chimera (33). Structure superposition and representation were performed with PyMOL (DeLano Scientific), and root mean square deviation calculation with LSQMAN (Uppsala Software Factory). Electrostatic surface calculation was done with CCP4mg (34). Buried surface areas were calculated using AREAIMOL (34).

Pulldown Experiments—Yeast cells from log-phase cultures were vortexed with glass beads (4 × 3 min) in lysis buffer (50 mM Tris-HCl (pH 7.5), 300 mM NaCl, 5% glycerol, 0.2% Triton X-100, and 1 mM DTT). The lysate was cleared by centrifugation (13,200 rpm, 20 min) and used for pulldown experiments. Equimolar amounts of proteins were incubated with constant amounts of yeast extracts and 50 μl of amylose resin for 20 min in lysis buffer, followed by five wash steps with 1 ml of lysis buffer and elution with 35 μl of elution buffer (lysis buffer and 10 mM maltose). One-third of the elution volume was analyzed by SDS-PAGE and Western blotting with anti-Myc antibody.

Quantification of Western Blots against Myc-tagged Kar9p (myc-Kar9p)—For quantification, Western blots of three independent experiments were analyzed using the LAS-3000 mini-system and Multi Gauge software (FUJIFILM). Background signals from MBP lanes were subtracted from respective Western blot signals. Subsequently, individual Bim1p-MBP signals were normalized with the signal of MBP alone. Signals of coprecipitated Kar9p were compared with each other.

RESULTS

Crystal Structure of Bim1p EB1 Motif—We solved the crystal structure of the EB1 motif of Bim1p (Bim1p(C-term), amino acids 182–282) (supplemental Fig. S1) at 2.45 Å resolution (Table 1). The structure reveals a dimer, in which each monomer consists of a long and a short α-helix (Fig. 1*A*). The loop region connecting both helices contains a Bim1p-specific sequence insertion (*red boxed* sequence in supplemental Fig. S1), which was not visible in the electron density and thus is likely disordered. A kink in the lower third of the long helix induces asymmetry that is responsible for a root mean square deviation between both monomers of 1.60 Å. The hydrophobic dimerization interface involves a large buried surface of 1987 $Å^2$, suggesting stable dimerization in solution (supplemental Table S1).

An overlay of the structures of Bim1p and human EB1 (Protein Data Bank code 1WU9) showed that they adopt a similar overall fold (root mean square deviation of 1.2 Å) (supplemental Fig. S2*A*). However, the large helix of Bim1p is about

TABLE 1

Crystallographic data collection and refinement statistics

The resolution range of the last shell was 2.59–2.45 Å. ESRF, European Synchrotron Radiation Facility; r.m.s.d., root mean square deviation.

	Data set	
	Native	**Pt peak**
Data collection		
X-ray source (ESRF)	ID-29	ID-29
Space group	$P2_1$	$P2_1$
Cell symmetry	$a = 28.00$, $b = 42.5$, $c = 100.5$ Å; $\alpha = \gamma = 90$, $\beta = 90.3°$	$a = 28.00$, $b = 44.25$, $c = 101.25$ Å; $\alpha = \gamma = 90$, $\beta = 94.7°$
Wavelength (Å)	1.254	1.071
Data range (Å)	20–2.45	50–2.1
Observations (unique)	31,883 (8832)	90,864 (30,751)
$I/\sigma I$ (last shell)	13.12 (2.07)	8.16 (1.71)
Completeness (%) (last shell)	98.8 (98.3)	99.0 (63.8)
R_{sym} (last shell)[a]	7.8 (71.7)	14.2 (98.5)
Refinement		
R_{work} (R_{free})[b,c]	0.211 (0.240)	
r.m.s.d.	0.0098	
Bond lengths (Å)		
Bond angles	1.18°	
Ramachandran plot (%)		
Allowed	97.0	
Additionally allowed	1.8	
Outliers	1.2	

[a] R_{sym} is the unweighted R-value on I between symmetry mates.
[b] $R_{work} = \sum_{hkl}||F_o(hkl)| - |F_c(hkl)||/\sum_{hkl}|_o(hkl)|$ for reflections in the working data set.
[c] R_{free} = cross validation R-factor for 5% of reflections against which the model was not refined.

one-third longer than that in EB1 (total length of ~93 *versus* ~63 Å).

The EB1 motif of Bim1p contains few regions of pronounced surface charges (Fig. 1*B*). The plot of a sequence alignment (supplemental Fig. S1) onto the surface of the structure shows a region in the center of the dimer with high conservation (Fig. 1*C*). This conserved surface contains two regions with rather small hydrophobic patches. For EB1, these regions have been shown to mediate binding to cargo (12, 13, 35).

Structure of Bim1p C Terminus in Solution—Molecular weight analyses from small-angle x-ray scattering experiments revealed that Bim1p(C-term) and full-length Bim1p (Bim1p(FL)) also form dimers in solution (Fig. 1*D*). An overlay of the experimental scattering curve of Bim1p(C-term) with the calculated scattering curve from the crystal structure shows an almost perfect match (supplemental Fig. S2*B*). Thus, the dimer of the crystal structure is likely physiologic. Together, these results suggest that the EB1 motif mediates dimerization of Bim1p(FL). Because full-length human EB1 is also dimeric (36), this seems to be a general feature of this protein class.

Post-translational Modifications of Kar9p or Cofactors Are Required for Complex Formation with Bim1p—To assess complex formation between Bim1p and Kar9p, we performed pulldown experiments with both proteins recombinantly expressed in *E. coli*. Surprisingly, no direct interaction was observed. However, when we performed these experiments with recombinant Bim1p and extracts of Myc-Kar9p-expressing yeast cells, we clearly detected Kar9p in Western blots (Fig. 1*E*). These data suggest that post-translational modifications in Kar9p or cofactors are required for their interaction. The observation that Bim1p(FL) bound more efficiently to Kar9p than Bim1p(C-term) further indicates that regions outside the EB1 motif of Bim1p might contribute to the complex formation with Kar9p.

Kar9p Binding by Mutant Versions of Bim1p—To determine whether the yeast-specific loop region of 24 amino acids is important for complex formation with Kar9p, we generated Bim1p mutants with deletions of 12 or 14 amino acids in the loop (Bim1pΔ12 or Bim1pΔ14). Pulldown experiments with these recombinantly expressed mutants showed normal interactions with Kar9p (Fig. 2*A*), suggesting that the loop is dispensable for this function.

We used our structure and previously reported mutations in EB1 to generate point-mutated versions of Bim1p(FL) and performed pulldown experiments with extracts from Myc-Kar9p-expressing cells, followed by Western blotting. Among the 15 mutant Bim1p(FL) proteins that were soluble, we found mutations R217A, F219A, Y220A, F221A, E228A, and H232A to impair Kar9p binding (Fig. 2, *B* and *C*). In contrast, the Bim1p mutations E214A, E218A, and N222A enhanced Kar9p binding. Pulldown experiments with a subset of mutations in Bim1p(C-term) followed by quantitative analyses of Western blots revealed consistent results, with the exception of mutations I227A and R225A (Fig. 2, *C–E*).

When plotting the interaction-modulating mutations onto the surface of the Bim1p(C-term) structure, a patch within the highly conserved hydrophobic core is observed (compare supplemental Fig. S2, *C* and *D*, with Fig. 1*C*). We also compared these residues with the amino acids identified in EB1 to influence cargo binding (12, 13, 35). Several of the corresponding residues in both proteins are identical, and others lie in close vicinity (supplemental Fig. S3), suggesting that their overall mode of interaction is similar. However, human EB1 failed in pulldown assays to interact with Myc-Kar9p from yeast extracts (Fig. 2, *C* and *D*). Thus, both proteins seem to bind in a somewhat different manner.

In Vivo Effects of Structure-based Mutations in Bim1p—Next, we tested selected Bim1p mutants in otherwise *BIM1* deletion strains by challenging them with increasing concentrations of the microtubule-depolymerizing fungicide benomyl or at increased temperatures. Similar to a previous report (6), the experimental readout for both assays was colony growth on agar plates.

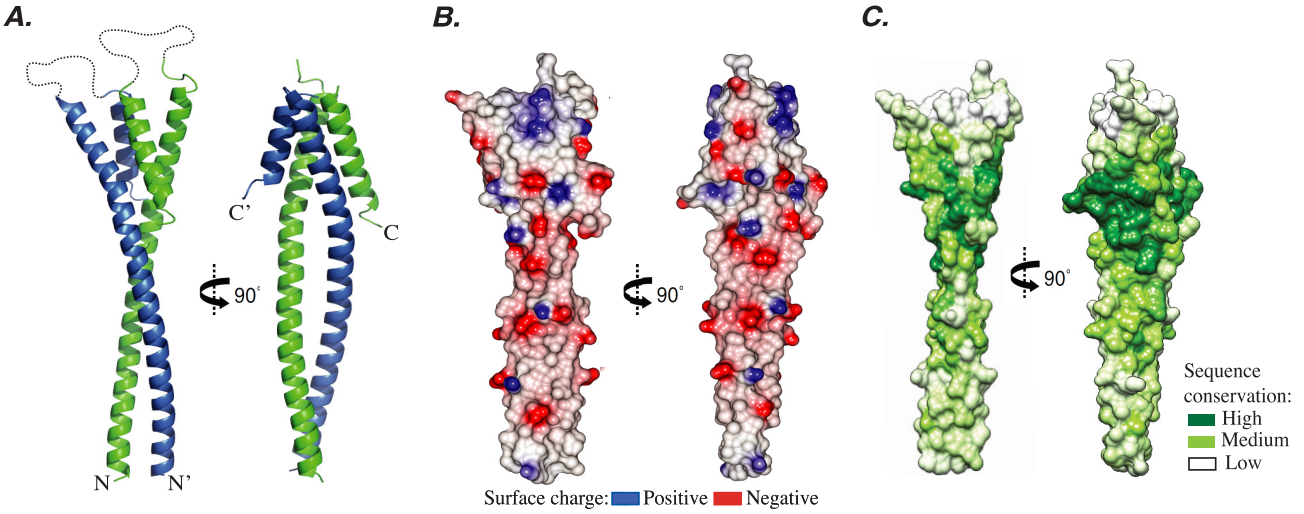

D.

Protein	Buffer	conc.	Rg	MW theor.	MW exp.
Bim1p (C-term)	10mM Hepes pH7.5 150mM NaCl 1mM EDTA 2mM DTT	4.4 mg/ml	2.95 nm	20 kDa	19 kDa
	50mM Sodium-phosphate pH7.5 150mM NaCl 1mM EDTA 2mM DTT	4.7 mg/ml	2.98 nm	20 kDa	23 kDa
Bim1p (FL)	10mM Hepes pH7.5 500mM NaCl 1mM EDTA 2mM DTT	1.3 mg/ml	5.89 nm	76 kDa	72 kDa
	50mM Sodium-phosphate pH7.5 500mM NaCl 1mM EDTA 2mM DTT	1.1 mg/ml	5.87 nm	76 kDa	74 kDa

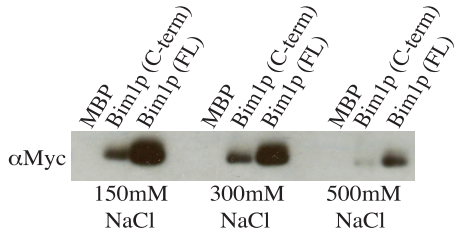

FIGURE 1. **Function and structure of Bim1p C-terminal EB1 motif.** *A–C*, structural analyses of the C-terminal EB1 motif of Bim1p. *A*, ribbon representation of the crystal structure shows that Bim1p(C-term) forms a coiled-coil dimer (monomers in *blue* and *green*). N and C termini are marked *N* and *C*, respectively. *Dotted lines* indicate positions of a loop region not visible in electron density. *B*, representation of surface charges of Bim1p(C-term). *C*, surface representation of sequence conservation (for alignment, see supplemental Fig. S1). *D*, molecular weight measurements by small-angle x-ray scattering confirmed that Bim1p(FL) and Bim1p(C-term) are dimeric in solution. *E*, amylose pulldown experiments with recombinant MBP-tagged Bim1p and yeast extracts expressing Myc-Kar9p, followed by Western blotting against Myc. Bim1p(FL) bound more efficiently to Kar9p compared with Bim1p(C-term).

Although we did not observe growth defects at 37 °C with any of the tested *bim1* mutants, sensitivity to treatment with benomyl was increased in a yeast strain expressing the Bim1p(F219A) mutant (Fig. 2*E* and supplemental Fig. S4*A*). In our pulldown assays, this mutation had almost completely lost its interaction with Kar9p (Fig. 2, *C–E*). Mutations without defects in pulldown experiments also failed to show effects in both *in vivo* assays. Interestingly, the Bim1p(I229A) mutant, which yielded a normal Kar9p interaction in pulldown assays (Fig. 2, *C* and *E*) displayed a lower benomyl sensitivity compared with wild-type Bim1p (Fig. 2*E* and supplemental Fig. S4*A*). The fact that not all mutations with reduced Kar9p binding yield growth defects suggests that complex assembly might be more robust *in vivo*. It is also consistent with the presence of a second, partially redundant Kar9p-binding site in Bim1p.

Bim1p Linker Region Contributes to Kar9p Binding—Indeed, the better binding of Bim1p(FL) compared with Bim1p(C-term) (Fig. 1*E*) suggests a contribution of regions outside the EB1 motif to Kar9p interaction. On the other hand, deletion of the EB1 motif or larger C-terminal fragments resulted in a loss of Kar9p binding (Fig. 3, *A* and *B*), arguing against a second binding region.

Because deletion of the EB1 motif is likely to abolish dimerization of Bim1p, we also tested the possibility that this feature is required for a potential second binding site. We replaced the EB1 motif with the dimerization-mediating coiled-coil region of GCN4 (Fig. 3*A*) and tested these mutants in pulldown experiments. Indeed, we could pull down Myc-Kar9p with a protein consisting of Bim1p amino acids 1–187 fused to GCN4 (Bim1p(1–187)-GCN4) (Fig. 3, *A* and *B*). This

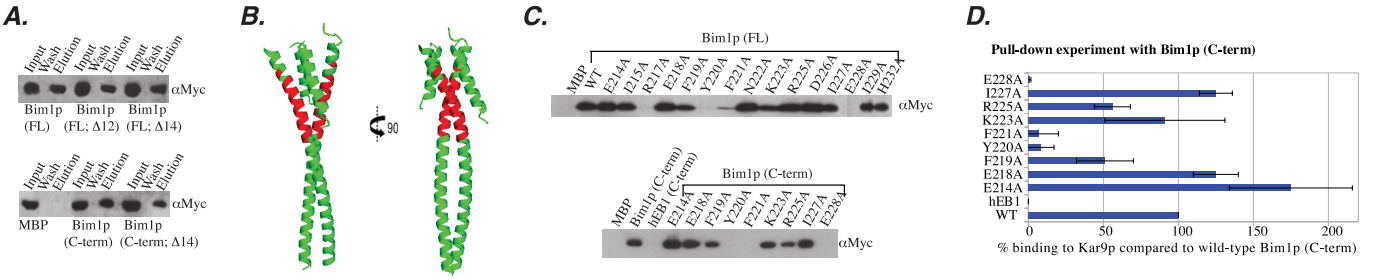

E.

Mutation	Bim1p (FL) Purification	Bim1p (C-term) Purification	Effect in pulldown experiments	Expression in yeast	Temperature-sensitivity	Benomyl-supersensitivity
E214A	x	x	enhanced binding	x	no effect	no effect
I215A	x		no effect			
E216A	degradation		-			
R217A	x		reduced binding	x	no effect	no effect
E218A	x	x	slightly enhanced binding			
F219A	x	x	reduced binding	x	no effect	sensitive at 12.5mg
Y220A	x	x	reduced binding			
F221A	x	x	reduced binding	x	no effect	no effect
N222A	x		enhanced binding			
K223A	x	x	no effect			

Mutation	Bim1p (FL) Purification	Bim1p (C-term) Purification	Effect in pulldown experiments	Expression in yeast	Temperature-sensitivity	Benomyl-supersensitivity
L224A	degradation		-			
R225A	x	x	reduced binding			
D226A	x		no effect			
I227A	x	x	enhanced binding (C-term) normal binding (FL)			
E228A	x	x	no binding	x	no effect	no effect
I229A	x		normal binding	x	no effect	less sensitive
H232A	x		reduced binding			
T275A	degradation		-			
E277A	degradation		-			
F279A	degradation		-			

FIGURE 2. **Characterization of structure-based Bim1p mutations.** *A*, pulldown experiments with Bim1p containing loop deletions and yeast extracts showed no defects in Kar9p binding. *B*, structural model with regions subjected to point mutations highlighted in *red* (see also supplemental Fig. S2, *C* and *D*). *C*, pulldown experiments with mutant Bim1p and yeast extracts. *D*, graph summarizing the quantification of three independent pulldown experiments. *E*, summary of pulldown experiments shown in *C* and *D* as well as growth sensitivity of Bim1p mutants *in vivo* upon treatment with benomyl or increased temperature (supplemental Fig. S4*A*).

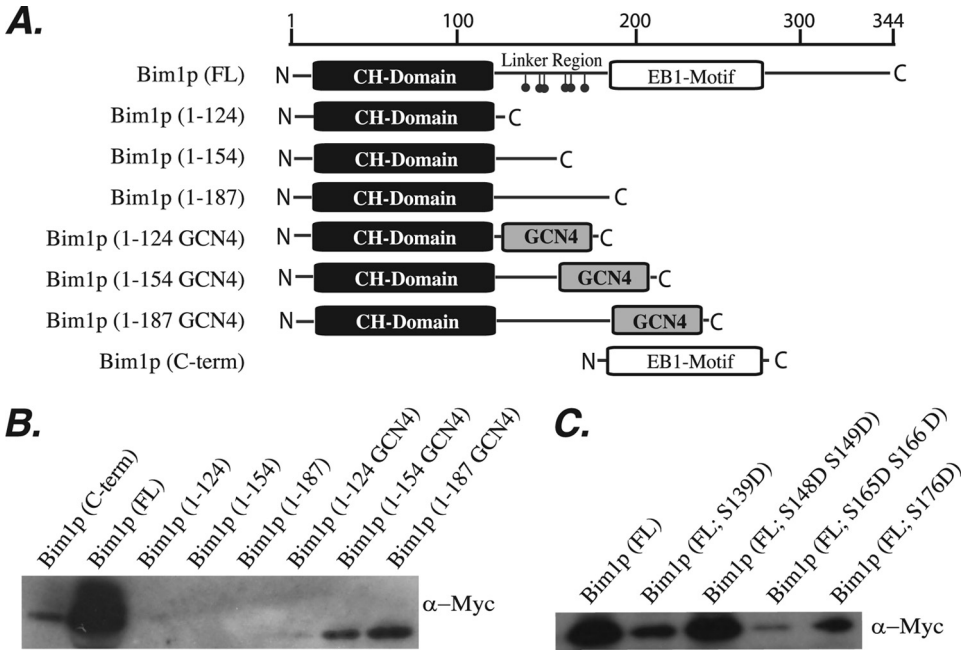

FIGURE 3. **Bim1p linker region contains previously undetected Kar9p-binding region that is regulated by phosphorylation.** *A*, schematic of Bim1p mutants. *B*, pulldown experiments with recombinant Bim1p mutants and yeast extracts. Bim1p lacking the EB1 motif only interacted with Kar9p when fused to the GCN4 dimerization domain. *C*, pulldown experiments with Aurora B/Ipl1p-phosphomimetic mutants of Bim1p yielded severely reduced complex formation with Kar9p.

interaction became weaker when parts of the Bim1p linker region were deleted (Fig. 3, *A* and *B*), suggesting that a region between the CH domain and the EB1 motif mediates binding to Kar9p and that this function requires Bim1p dimerization. A rescue experiment with Bim1p(1–187)-GCN4 in the Δ*bim1* background only slightly alleviated growth defects (supplemental Fig. S4*B*), which is consistent with the observation that either Bim1p(1–187)-GCN4 or the EB1 motif alone binds to Kar9p significantly less efficiently compared with Bim1p(FL) (Fig. 1*E* and Fig. 3, *A* and *B*).

Aurora B-dependent Phosphorylation of Bim1p Impairs Kar9p Binding—The novel Kar9p-binding region between the CH domain and EB1 motif is phosphorylated during anaphase at six serines (positions 139, 148, 149, 165, 166, and 176) by the Aurora B kinase Ipl1p (Fig. 3*A*) (16) and is required for proper spindle mid-zone disassembly. Mutations of these serines to glutamic acids efficiently mimic phosphorylation of Bim1p (16).

We tested whether phosphorylation of Bim1p affects its association with Kar9p by performing pulldown experiments with phosphomimetic mutants in the linker region of Bim1p.

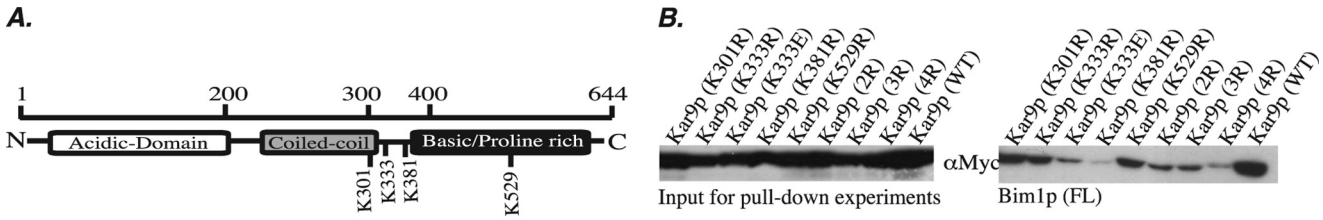

C.

Mutation	Effect in pull-down with Bim1p (FL)	Temperature-sensitivity	Benomyl-supersensitivity
Kar9p (WT)	normal binding	slightly sensitive at 30°C and 37°C	highly sensitive at 2.5μg and 5μg
Kar9p (K301R)	slightly reduced binding	slightly sensitive at 30°C and 37°C	highly sensitive at 2.5μg and 5μg
Kar9p (K333R)	slightly reduced binding	slightly sensitive at 30°C and 37°C	less sensitive at 2.5μg and 5μg than compared to WT
Kar9p (K333E)	strongly reduced binding	slightly sensitive at 30°C and 37°C	no sensitivity at 2.5μg and less sensitivity at 5μg and 7.5μg compared to WT
Kar9p (K381R)	strongly reduced binding	slightly sensitive at 30°C and 37°C	highly sensitive at 2.5μg and 5μg
Kar9p (K529R)	slightly reduced binding	slightly sensitive at 30°C and 37°C	highly sensitive at 2.5μg and 5μg
Kar9p (2R)	reduced binding	slightly sensitive at 30°C and 37°C	more sensitive at 2.5μg than compared to WT
Kar9p (3R)	reduced binding	slightly sensitive at 30°C and 37°C	less sensitivity at 2.5μg and at 5μg compared to WT
Kar9p (4R)	strongly reduced binding	slightly sensitive at 30°C and 37°C	less sensitivity at 2.5μg and at 5μg compared to WT

FIGURE 4. **Sumoylation of Kar9p is prerequisite for complex formation with Bim1p.** *A*, schematic drawing of the domain architecture of Kar9p with its sumoylation sites Lys-301, Lys-333, Lys-381, and Lys-529. *B*, pulldown experiments with recombinant Bim1p(FL) and extracts from strains expressing mutant Kar9p followed by Western blotting against Myc-Kar9p showed significantly reduced binding to Bim1p. *C*, summary of the benomyl and temperature sensitivity of yeast cells expressing sumoylation-deficient Kar9p (supplemental Fig. S5) and corresponding pulldown experiments (*B*).

Indeed, a strongly reduced interaction was observed with the double mutant Bim1p(FL;S165D/S166D) (Fig. 3*C*). With Bim1p(FL;S139D) and Bim1p(FL;S176D), a more moderate reduction of Kar9p association was observed. These data indicate that Aurora B/Ipl1p-dependent phosphorylation of Bim1p might regulate the binding to Kar9p via the Bim1p linker region. This interpretation is consistent with the observation that Aurora B/Ipl1p kinase-dependent phosphorylation of Bim1p is required for normal progression of mitosis (16).

Kar9p Sumoylation Is Required for Bim1p Binding—Kar9p is sumoylated at Lys-301, Lys-333, Lys-381, and Lys-529 (18). A yeast strain expressing a Kar9p version with all four sumoylation sites mutated fails to accumulate Kar9p asymmetrically on the mother-directed spindle pole body and emanating astral microtubules (18). Because sumoylation is hardly detectable in G_1 phase but is well established during metaphase, this modification was proposed to have a positive effect on the function of Kar9p during mitosis (18).

We tested the effect of Kar9p sumoylation on its interaction with Bim1p by generating yeast strains with point mutations in sumoylation sites of Kar9p (Fig. 4*A*). These Myc-Kar9p mutants were tested in pulldown experiments for an interaction with recombinant MBP-Bim1p. We observed an almost complete loss of Bim1p(FL) binding when all four sumoylation sites were mutated (Kar9p(4R)) and more moderate defects when only two or three sites were mutated (Kar9p(2R), K301R/K381R; and Kar9p(3R), K301R/K381R/K529R) (Fig. 4*B*). With the exception of K381R, defects in Bim1p association upon mutation of individual sumoylation sites in Kar9p were more moderate compared with those upon multiple mutations. Pulldown experiments with His-tagged Smt3p followed by Western blotting with anti-Myc antibody revealed that Myc-Kar9p was indeed sumoylated in our extracts and that this modification was reduced upon mutation of multiple sumoylation sites (supplemental Fig. S5*B*). Thus, sumoylation at K381R and perhaps at additional sites of Kar9p seems to be required for efficient complex formation with Bim1p.

Effects of Kar9p Sumoylation on Cell Growth—To study the importance of individual Kar9p sumoylation sites *in vivo*, we overexpressed sumoylation mutant versions of Kar9p under the control of a *GAL1* promoter in a *KAR9* deletion background and tested them for benomyl and temperature sensitivity. Already, the overexpression of wild-type Kar9p resulted in considerable growth defects (Fig. 4*C*; compare supplemental Fig. S5 with supplemental Fig. S4*A*). We reasoned that less active Kar9p mutants might produce weaker dominant-negative effects, offering a simple approach to unambiguously assess defects in Kar9p function. Indeed, the observed growth defects of strains with single Kar9p mutations correlated well with the defects in the pulldown experiments (Fig. 4*C* and supplemental Fig. S5). Whereas Kar9p(2R) showed growth defects with similar strength as wild-type Kar9p, the Kar9p(3R) and Kar9p(4R) mutants caused significantly smaller growth defects (Fig. 4*C* and supplemental Fig. S5).

DISCUSSION

Leisner *et al.* (18) showed that sumoylation occurs during metaphase and that Kar9p(4R) fails to localize to only one of the spindle pole bodies. It was further shown that the Bim1p-Kar9p complex assembles before loading onto the microtubules via the spindle pole bodies (37). Here, we have demonstrated that Kar9p sumoylation is important for complex formation with Bim1p. In agreement with the previous studies, our findings therefore suggest that sumoylation induces assembly of the early spindle orientation complex. We should note that our experiments do not rule out the possibility that additional factors may be required for this interaction. Furthermore, Western blotting with anti-Smt3p antibody after Bim1p pulldown experiments suggested additional, previously undetected sumoylation sites in Kar9p.[3] Their importance remains to be investigated in future studies. Notably, strong defects of mutant proteins in pulldown experiments often translated into much weaker defects *in vivo*. This suggests either that the dynein-dependent spindle elongation compensates for these defects or that other countervailing mechanisms exist.

Phosphorylation of the linker region of Bim1p by the Aurora B/Ipl1p kinase occurs at the beginning of anaphase (16). This is the time point when spindle orientation is completed and the Myo2p-Kar9p-Bim1p complex has to disassemble. We have shown that phosphomimetic mutations in our newly identified Kar9p interaction site of Bim1p result in reduced complex formation. Therefore, our data suggest a cell cycle-dependent inactivation of the Bim1p-Kar9p interaction by phosphorylation of Bim1p in the linker region. A working model of the cell cycle-dependent assembly and disassembly of the Myo2p-Kar9p-Bim1p complex is given in supplemental Fig. S6.

It has recently been reported that binding of human EB1 to Aurora B kinase protects it from inactivation (17). In this context, it would be interesting to see whether phosphorylated EB1 or Bim1p shows increased binding to Aurora B/Ipl1p kinase, thereby protecting it from inactivation. If true, this feedback loop could constitute a novel entry point for inhibitory approaches.

Acknowledgments—We thank Sigrun Jaklin and Stephane Roche for contributions and Stefan Jentsch for providing the His-Smt3p plasmid. We acknowledge support from the crystallization facility of the Max Planck Institute of Biochemistry and the European Synchrotron Radiation Facility for provision of synchrotron radiation facilities.

REFERENCES

1. Yin, H., Pruyne, D., Huffaker, T. C., and Bretscher, A. (2000) Myosin V orients the mitotic spindle in yeast. *Nature* **406,** 1013–1015
2. Liakopoulos, D., Kusch, J., Grava, S., Vogel, J., and Barral, Y. (2003) Asymmetric loading of Kar9 onto spindle poles and microtubules ensures proper spindle alignment. *Cell* **112,** 561–574
3. Miller, R. K., and Rose, M. D. (1998) Kar9p is a novel cortical protein required for cytoplasmic microtubule orientation in yeast. *J. Cell Biol.* **140,** 377–390
4. Nishisho, I., Nakamura, Y., Miyoshi, Y., Miki, Y., Ando, H., Horii, A., Koyama, K., Utsunomiya, J., Baba, S., and Hedge, P. (1991) Mutations of chromosome 5q21 genes in FAP and colorectal cancer patients. *Science* **253,** 665–669
5. Bienz, M. (2001) Spindles cotton on to junctions, APC and EB1. *Nat. Cell Biol.* **3,** E67–E68
6. Schwartz, K., Richards, K., and Botstein, D. (1997) *BIM1* encodes a microtubule-binding protein in yeast. *Mol. Biol. Cell* **8,** 2677–2691
7. Half, E., Bercovich, D., and Rozen, P. (2009) Familial adenomatous polyposis. *Orphanet J. Rare Dis.* **4,** 22
8. Orimo, T., Ojima, H., Hiraoka, N., Saito, S., Kosuge, T., Kakisaka, T., Yokoo, H., Nakanishi, K., Kamiyama, T., Todo, S., Hirohashi, S., and Kondo, T. (2008) Proteomic profiling reveals the prognostic value of adenomatous polyposis coli end-binding protein 1 in hepatocellular carcinoma. *Hepatology* **48,** 1851–1863
9. Dong, X., Liu, F., Sun, L., Liu, M., Li, D., Su, D., Zhu, Z., Dong, J. T., Fu, L., and Zhou, J. (2010) Oncogenic function of microtubule end-binding protein 1 in breast cancer. *J. Pathol.* **220,** 361–369
10. Hayashi, I., and Ikura, M. (2003) Crystal structure of the amino-terminal microtubule-binding domain of end-binding protein 1 (EB1). *J. Biol. Chem.* **278,** 36430–36434
11. Sandblad, L., Busch, K. E., Tittmann, P., Gross, H., Brunner, D., and Hoenger, A. (2006) The *Schizosaccharomyces pombe* EB1 homolog Mal3p binds and stabilizes the microtubule lattice seam. *Cell* **127,** 1415–1424
12. Slep, K. C., Rogers, S. L., Elliott, S. L., Ohkura, H., Kolodziej, P. A., and Vale, R. D. (2005) Structural determinants for EB1-mediated recruitment of APC and spectraplakins to the microtubule plus-end. *J. Cell Biol.* **168,** 587–598
13. Honnappa, S., John, C. M., Kostrewa, D., Winkler, F. K., and Steinmetz, M. O. (2005) Structural insights into the EB1-APC interaction. *EMBO J.* **24,** 261–269
14. Miller, R. K., Cheng, S. C., and Rose, M. D. (2000) Bim1p/Yeb1p mediates the Kar9p-dependent cortical attachment of cytoplasmic microtubules. *Mol. Biol. Cell* **11,** 2949–2959
15. Slep, K. C., and Vale, R. D. (2007) Structural basis of microtubule plus-end tracking by XMAP215, CLIP-170, and EB1. *Mol. Cell* **27,** 976–991
16. Zimniak, T., Stengl, K., Mechtler, K., and Westermann, S. (2009) Phosphoregulation of the budding yeast EB1 homolog Bim1p by Aurora/Ipl1p. *J. Cell Biol.* **186,** 379–391
17. Sun, L., Gao, J., Dong, X., Liu, M., Li, D., Shi, X., Dong, J. T., Lu, X., Liu, C., and Zhou, J. (2008) EB1 promotes Aurora B kinase activity through blocking its inactivation by protein phosphatase 2A. *Proc. Natl. Acad. Sci. U.S.A.* **105,** 7153–7158
18. Leisner, C., Kammerer, D., Denoth, A., Britschi, M., Barral, Y., and Liakopoulos, D. (2008) Regulation of mitotic spindle asymmetry by SUMO and the spindle assembly checkpoint in yeast. *Curr. Biol.* **18,** 1249–1255
19. Meednu, N., Hoops, H., D'Silva, S., Pogorzala, L., Wood, S., Farkas, D., Sorrentino, M., Sia, E., Meluh, P., and Miller, R. K. (2008) The spindle-positioning protein Kar9p interacts with the sumoylation machinery in *Saccharomyces cerevisiae*. *Genetics* **180,** 2033–2055
20. Maekawa, H., Usui, T., Knop, M., and Schiebel, E. (2003) Yeast Cdk1 translocates to the plus-end of cytoplasmic microtubules to regulate bud cortex interactions. *EMBO J.* **22,** 438–449
21. Adams, A., Gottschling, D. E., Kaiser, C. A., and Stearns, T. (1997) *Methods in Yeast Genetics*, Cold Spring Harbor Laboratory Press, Cold Spring Harbor, NY
22. Gietz, R. D., and Schiestl, R. H. (1991) Applications of high efficiency lithium acetate transformation of intact yeast cells using single-stranded nucleic acids as carrier. *Yeast* **7,** 253–263
23. Gietz, R. D., and Sugino, A. (1988) New yeast-*Escherichia coli* shuttle vectors constructed with *in vitro* mutagenized yeast genes lacking 6-base pair restriction sites. *Gene* **74,** 527–534
24. Knop, M., Siegers, K., Pereira, G., Zachariae, W., Winsor, B., Nasmyth, K., and Schiebel, E. (1999) Epitope tagging of yeast genes using a PCR-based strategy: more tags and improved practical routines. *Yeast* **15,** 963–972
25. Heuck, A., Fetka, I., Brewer, D. N., Hüls, D., Munson, M., Jansen, R. P., and Niessing, D. (2010) The structure of the Myo4p globular tail and its function in *ASH1* mRNA localization. *J. Cell Biol.* **189,** 497–510
26. Heuck, A., Du, T. G., Jellbauer, S., Richter, K., Kruse, C., Jaklin, S., Müller, M., Buchner, J., Jansen, R. P., and Niessing, D. (2007) Monomeric myosin

[3] D. Hüls, Z. Storchova, and D. Niessing, unpublished data.

V uses two binding regions for the assembly of stable translocation complexes. *Proc. Natl. Acad. Sci. U.S.A.* **104,** 19778–19783
27. Graebsch, A., Roche, S., and Niessing, D. (2009) X-ray structure of Pur-α reveals a Whirly-like fold and an unusual nucleic acid-binding surface. *Proc. Natl. Acad. Sci. U.S.A.* **106,** 18521–18526
28. Kabsch, W. (1993) Automatic processing of rotation diffraction data from crystals of initially unknown symmetry and cell constants. *J. Appl. Crystallogr.* **26,** 795–800
29. Sheldrick, G. M. (2008) A short history of SHELX. *Acta Crystallogr. A* **64,** 112–122
30. Emsley, P., and Cowtan, K. (2004) Coot: model-building tools for molecular graphics. *Acta Crystallogr. D Biol. Crystallogr.* **60,** 2126–2132
31. McCoy, A. J., Grosse-Kunstleve, R. W., Adams, P. D., Winn, M. D., Storoni, L. C., and Read, R. J. (2007) Phaser crystallographic software. *J. Appl. Crystallogr.* **40,** 658–674
32. Bricogne, G., Blanc, E., Brandl, M., Flensburg, C., Keller, P., Paciorek, P., Roversi, P., Sharff, A., Smart, O., Vonrhein, C., and Womack, T. (2010) *BUSTER*, Global Phasing Ltd., Cambridge, United Kingdom
33. Pettersen, E. F., Goddard, T. D., Huang, C. C., Couch, G. S., Greenblatt, D. M., Meng, E. C., and Ferrin, T. E. (2004) UCSF Chimera–a visualization system for exploratory research and analysis. *J. Comput. Chem.* **25,** 1605–1612
34. Collaborative Computational Project, Number 4 (1994) The CCP4 suite: programs for protein crystallography. *Acta Crystallogr. D Biol. Crystallogr.* **50,** 760–763
35. Honnappa, S., Gouveia, S. M., Weisbrich, A., Damberger, F. F., Bhavesh, N. S., Jawhari, H., Grigoriev, I., van Rijssel, F. J., Buey, R. M., Lawera, A., Jelesarov, I., Winkler, F. K., Wüthrich, K., Akhmanova, A., and Steinmetz, M. O. (2009) An EB1-binding motif acts as a microtubule tip localization signal. *Cell* **138,** 366–376
36. Buey, R. M., Mohan, R., Leslie, K., Walzthoeni, T., Missimer, J. H., Menzel, A., Bjelic, S., Bargsten, K., Grigoriev, I., Smal, I., Meijering, E., Aebersold, R., Akhmanova, A., and Steinmetz, M. O. (2011) Insights into EB1 structure and the role of its C-terminal domain for discriminating microtubule tips from the lattice. *Mol. Biol. Cell* **22,** 2912–2923
37. Cuschieri, L., Miller, R., and Vogel, J. (2006) γ-Tubulin is required for proper recruitment and assembly of Kar9-Bim1 complexes in budding yeast. *Mol. Biol. Cell* **17,** 4420–4434